Unsupervised Machine Learning and Band Topology

Mathias S. Scheurer[1] and Robert-Jan Slager[1,2]
[1]Department of Physics, Harvard University, Cambridge, Massachusetts 02138, USA
[2]TCM Group, Cavendish Laboratory, University of Cambridge, J. J. Thomson Avenue, Cambridge CB3 0HE, United Kingdom

(Received 10 January 2020; accepted 15 May 2020; published 1 June 2020)

The study of topological band structures is an active area of research in condensed matter physics and beyond. Here, we combine recent progress in this field with developments in machine learning, another rising topic of interest. Specifically, we introduce an unsupervised machine learning approach that searches for and retrieves paths of adiabatic deformations between Hamiltonians, thereby clustering them according to their topological properties. The algorithm is general, as it does not rely on a specific parametrization of the Hamiltonian and is readily applicable to any symmetry class. We demonstrate the approach using several different models in both one and two spatial dimensions and for different symmetry classes with and without crystalline symmetries. Accordingly, it is also shown how trivial and topological phases can be diagnosed upon comparing with a generally designated set of trivial atomic insulators.

DOI: 10.1103/PhysRevLett.124.226401

Introduction.—With the advent of the concept of topological insulators [1,2], considerable research effort has focused on further underpinning the theoretical understanding and material realizations of such nontrivial systems. In the past two years, specific progress has been made on systematically categorizing topological band structures upon considering the role of crystal symmetries [3,4]. The different topological band structures, that is, configurations that cannot be mapped into each other without closing the gap and breaking the symmetries under considerations, are obtained as solutions to a combinatorial problem [5], matching the underlying descriptive equivariant K theory [5,6].

Another active research field is applying machine learning (ML) techniques to physics [7–10]. There are many applications, such as providing variational representations of wave functions [11,12], acceleration of Monte Carlo sampling [13], in material science and density-functional theory [14–20], and detection of phase transitions [21–45]. Concerning the latter, it has been established that topological phase transitions are generally more difficult to capture than symmetry-breaking phase transitions [46], due to the absence of a local order parameter. While some progress has been achieved, most approaches for learning topological phases rely on supervised learning (require labeled data) and/or manual feature engineering taking into account prior knowledge of the phases. In [35], however, an unsupervised ML approach was proposed to classify samples based on topological properties from raw data. The key idea is to view the samples as nodes on a graph with connections defined by the local similarity $K_{l,l'}$ of pairs l, l' of samples. The global structure of the graph can be represented in a low-dimensional embedding constructed from diffusion maps [47]; this, in turn, reveals the distinct topological classes.

When detecting "bulk topological order" [48], e.g., of two-dimensional (2D) XY models, this procedure can be directly applied to (Monte Carlo) snapshots [35], revealing the presence or absence of superselection sectors [49]. In this Letter, we are interested in band topology. We are then typically given a few Hamiltonians, our "samples," represented by the dark blue and red dots in Fig. 1(a), that we want to cluster according to whether they can be deformed into each other. These do not *a priori* cover the entire space of Hamiltonians of that symmetry class. To make sure we are not missing any paths, we could randomly sample Hamiltonians of that symmetry class (light dots), as suggested recently within a different ML setup [45], and apply the procedure of [35] to this larger set of samples. Since the amount of random samples grows rapidly with the size of the Hilbert space, we here propose a different ML procedure that goes beyond previous work by

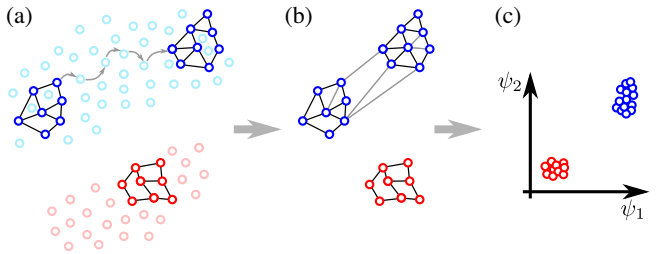

FIG. 1. Instead of randomly sampling Hamiltonians of a symmetry class [light red and blue dots in (a)], a path-finding algorithm is employed to retrieve adiabatic deformations (gray arrows) between Hamiltonians (dark red and blue dots). This constructs an effective graph (b), which we use to find a low-dimensional embedding (c) that reveals the topologically distinct classes.

explicitly searching for adiabatic paths (little gray arrows). In this way, we construct an effective graph, see Fig. 1(b), that we take as starting point, yielding a low-dimensional embedding [Fig. 1(c)] that reflects the topological sectors. In this space, we then apply k-means clustering.

Algorithm.—Suppose we are given a set of m translationally invariant Hamiltonians with N_b bands, $\{h^l_{\boldsymbol{k}} \in \mathbb{C}^{N_b \times N_b}, l = 1, \ldots, m\}$. Our goal is to classify the samples $l = 1, \ldots, m$ topologically, i.e., decide which Hamiltonians can be deformed into each other without closing the gap or breaking a certain subset of symmetries of the Hamiltonians. These can include time-reversal symmetry (TRS) Θ, particle-hole symmetry (PHS) Ξ, and chiral symmetry C, as in the Altland-Zirnbauer (AZ) classification, or any other set of unitary symmetries constituting a group $\mathcal{G}$.

To define a "continuous deformation," we introduce the following measure of $\boldsymbol{k}$-local similarity between Hamiltonians l and l' (N_k is the number of $\boldsymbol{k}$ points in the sum):

$$S_{l,l'} = \frac{1}{N_k}\sum_{\boldsymbol{k}} \frac{1}{N_b}\sum_{n=1}^{N_b} |\langle \psi^l_{n\boldsymbol{k}} | \psi^{l'}_{n\boldsymbol{k}} \rangle|^2, \tag{1}$$

with eigenstates $|\psi^l_{n\boldsymbol{k}}\rangle$, satisfying $h^l_{\boldsymbol{k}}|\psi^l_{n\boldsymbol{k}}\rangle = \epsilon^l_{n\boldsymbol{k}}|\psi^l_{n\boldsymbol{k}}\rangle$, $\epsilon^l_{n\boldsymbol{k}} < \epsilon^l_{n'\boldsymbol{k}}$ for $n < n'$ (for now, we neglect degeneracies). The normalization in Eq. (1) is chosen such that $S_{l,l} = 1$. It further holds $S_{l,l'} = S_{l',l}$, $0 \le S_{l,l'} \le 1$, and $S_{l,l'} = 1$ if and only if $h^l_{\boldsymbol{k}}$ and $h^{l'}_{\boldsymbol{k}}$ are identical except for a deformation of the band energies, that does not close any gap in the system. If the set of Hamiltonians already contains all relevant adiabatic paths, we can directly use the approach of [35] with connections $K^0_{l,l'} = \exp[-(1 - S_{l,l'})/\epsilon]$ to perform the topological analysis, where ϵ is a suitably chosen coarse-graining parameter. As discussed above, this is very unlikely. To overcome this issue, we use that the spectra of two Hamiltonians $h_{\boldsymbol{k}}$ and $h'_{\boldsymbol{k}}$ are topologically equivalent if $h'_{\boldsymbol{k}} = U_{\boldsymbol{k}} h_{\boldsymbol{k}} U^\dagger_{\boldsymbol{k}}$ with unitary $U_{\boldsymbol{k}} = e^{i\varphi_{\boldsymbol{k}}\Lambda}$ that respects the symmetries of the symmetry class under consideration; here Λ is the associated generator and $\varphi_{\boldsymbol{k}}$ is required to be a continuous function of $\boldsymbol{k}$. On the level of states, this "adiabatic deformation" corresponds to $|\psi_{n\boldsymbol{k}}\rangle \to U_{\boldsymbol{k}}|\psi_{n\boldsymbol{k}}\rangle$. For each pair of Hamiltonians l and l' in Eq. (1), we perform a sequence of deformations, $|\psi^{l'}_{n\boldsymbol{k}}\rangle \to |\psi^{l',1}_{n\boldsymbol{k}}\rangle \to |\psi^{l',2}_{n\boldsymbol{k}}\rangle \to \cdots \to |\psi^{l',N_f}_{n\boldsymbol{k}}\rangle$, to maximize the value of $S_{l,l'}$. The resultant final value $S^f_{l,l'}$ of the similarity measure, i.e., $S_{l,l'}$ with $|\psi^{l'}_{n\boldsymbol{k}}\rangle$ replaced by $|\psi^{l',N_f}_{n\boldsymbol{k}}\rangle$, will be used as input for $K_{l,l'} = \exp[-(1 - S^f_{l,l'})/\epsilon]$.

Before discussing our path-finding ML procedure, we revisit the issue of degeneracies and refine $S_{l,l'}$ in Eq. (1), allowing the possibility of keeping specific subsets of gaps open while others are permitted to close. Taking such different partitions of bands has recently been linked to new forms of topology [50–53]. To this end, we replace the kernel in Eq. (1) by the refined similarity measure

$$S_{l,l'} = \frac{1}{N_k}\sum_{\boldsymbol{k}} \frac{1}{\tilde{N}_b}\sum_{n=1}^{N_b}\sum_{n' \in \mathcal{S}_n} |\langle \psi^l_{n\boldsymbol{k}} | \psi^{l'}_{n'\boldsymbol{k}} \rangle|^2, \tag{2}$$

where $\mathcal{S}_n$ is the subset of bands $\{1, \ldots, N_b\}$ that band n is allowed to close gap or is degenerate with. Further, $\tilde{N}_b = \sum_{n=1}^{N_b} |\mathcal{S}_n|$ with $|\mathcal{S}_n|$ denoting the number of elements in $\mathcal{S}_n$. Our previous form in Eq. (1) corresponds to $\mathcal{S}_n = \{n\}$ with $|\mathcal{S}_n| = 1$. To illustrate this, consider the scenario of four bands, $n = 1$–4, assuming that we are only interested in the topological properties of the half filled gap, i.e., between $n = 2$ and $n = 3$, while the other gaps between $n = 1$ and $n = 2$ and between $n = 3$ and $n = 4$ can be closed (or are zero due to a degeneracy). In that case, we have $S_1 = S_2 = \{1, 2\}$ and $S_3 = S_4 = \{3, 4\}$.

Next, we discuss the approach to find the path between two Hamiltonians l and l'. To construct the unitary transformation $U_{\boldsymbol{k}} = e^{i\varphi_{\boldsymbol{k}}\Lambda}$ of the Markov chain of deformations of Hamiltonian l', we first randomly sample a Hermitian generator $\Lambda \in \mathbb{C}^{N_b \times N_b}$. We find the optimal momentum dependence of $\varphi_{\boldsymbol{k}}$ by expanding the change of the measure of similarity in Eq. (2) under $|\psi^{l'}_{n\boldsymbol{k}}\rangle \to U_{\boldsymbol{k}}|\psi^{l'}_{n\boldsymbol{k}}\rangle$ in $\varphi_{\boldsymbol{k}}$ to derive the gradient ascent expression

$$\varphi_{\boldsymbol{k}} = -\eta \frac{1}{\tilde{N}_b}\sum_{n=1}^{N_b}\sum_{n' \in \mathcal{S}_n} \mathrm{Im}[\langle \psi^l_{n\boldsymbol{k}} | \Lambda | \psi^{l'}_{n'\boldsymbol{k}} \rangle \langle \psi^{l'}_{n'\boldsymbol{k}} | \psi^l_{n\boldsymbol{k}} \rangle] \tag{3}$$

with learning rate $\eta \in \mathbb{R}^+$. To ensure that the deformation performed on the Hamiltonian is smooth, we only accept the update if the maximum gradient of $\varphi_{\boldsymbol{k}}$ in momentum space divided by the average value of $|\varphi_{\boldsymbol{k}}|$ is smaller than the cutoff $2/|\Delta\boldsymbol{k}|$, where $\Delta\boldsymbol{k}$ connects neighboring points on the $\boldsymbol{k}$-grid used. We also compute the overall smoothness of the states, $\min_{\boldsymbol{k},n} \sum_{n' \in \mathcal{S}_n} |\langle \psi^{l'}_{n\boldsymbol{k}} | \psi^{l'}_{n'\boldsymbol{k}+\Delta\boldsymbol{k}} \rangle|^2$. If it drops below 0.7, we abort and set $S_{l,l'} = 0$, see Supplemental Material [54].

Besides smoothness of transformations, we also need to make sure that the deformation parametrized by Λ and $\varphi_{\boldsymbol{k}}$ preserves the symmetries of interest. Let us first focus on unitary symmetries and denote the representation of $g \in \mathcal{G}$ in momentum and in the N_b-dimensional space of the Hamiltonian by $\mathcal{R}_v(g)$ and $\mathcal{R}_\psi(g)$, respectively. The constraint $\varphi_{\mathcal{R}_v^{-1}(g)\boldsymbol{k}} \mathcal{R}_\psi(g) \Lambda \mathcal{R}^\dagger_\psi(g) = \varphi_{\boldsymbol{k}}\Lambda$ can be imposed by symmetrization,

$$\Lambda\varphi_{\boldsymbol{k}} \to \frac{1}{|\mathcal{G}|}\sum_{g \in \mathcal{G}} \varphi_{\mathcal{R}_v^{-1}(g)\boldsymbol{k}} \mathcal{R}_\psi(g) \Lambda \mathcal{R}^\dagger_\psi(g), \tag{4}$$

where $|\mathcal{G}|$ denotes the number of elements of $\mathcal{G}$ [55].

We distinguish two manners of implementing this procedure: if we sum over the (discretized) Brillouin zone in Eq. (2) and compute $\varphi_{\boldsymbol{k}}$ for all $\boldsymbol{k}$, we can explicitly perform the symmetrization in Eq. (4). This is what we do in the one-dimensional (1D) examples. In higher dimensions, we can speed up the algorithm using that topological properties are encoded in the behavior of the Wilson operators [52,56,57] along 1D cuts that go through all high-symmetry points. Therefore, we can restrict the momenta $\boldsymbol{k}$ in Eqs. (1)–(3) to these cuts. Furthermore, if diagonalization is the most computationally expensive step, we can use the symmetries to restrict this path to symmetry-inequivalent momenta only [see, e.g., Fig. 4(a)]. To compute $\varphi_{\mathcal{R}_v^{-1}(g)\boldsymbol{k}}$ in Eq. (4) in that case, we use that the symmetry of the Hamiltonian implies that $\varphi_{\mathcal{R}_v^{-1}(g)\boldsymbol{k}}$ is given by Eq. (3) with Λ replaced by $\mathcal{R}_\psi(g)\Lambda\mathcal{R}_\psi^\dagger(g)$ on the right-hand side.

Finally, we discuss how to take into account the symmetries of AZ classes. Imposing chiral symmetry, $Ch_{\boldsymbol{k}}C^\dagger = -h_{\boldsymbol{k}}$, amounts to symmetrizing the generator $\Lambda \to (\Lambda + C\Lambda C^\dagger)/2$ right after sampling it. It is, thus, only left to analyze the case of either TRS or PHS. Focusing on the former (same applies to PHS), the associated constraint $\varphi_{\boldsymbol{k}}\Theta\Lambda\Theta^\dagger = -\varphi_{-\boldsymbol{k}}\Lambda$ is rectified by replacing $\varphi_{\boldsymbol{k}} \to (\varphi_{\boldsymbol{k}}\Lambda - \varphi_{-\boldsymbol{k}}\Theta\Lambda\Theta^\dagger)/2$. If we want to restrict the momentum points to an irreducible set, we do not have to compute both $\varphi_{\boldsymbol{k}}$ and $\varphi_{-\boldsymbol{k}}$: using the TRS of the system, the symmetrization can also be restated as $\varphi_{\boldsymbol{k}} \to \sum_{p=\pm}\varphi_{\boldsymbol{k}}^p\Lambda^p/2$, where $\Lambda^\pm = (\Lambda \pm \Theta\Lambda\Theta^\dagger)/2$ and $\varphi_{\boldsymbol{k}}^\pm$ are given by Eq. (3) with Λ replaced by $\Lambda^\pm$.

Usually, Hamiltonians studied have additional symmetries beyond the subset of interest; in that case, the reliability is increased when performing initial "kicks": unless the two samples l and l' are already close according to the measure in Eq. (2), we sample a few random, $\boldsymbol{k}$-independent unitary transformations U_j, $j = 1, 2, \ldots N_{\text{kick}}$ (properly symmetrized) and take the one that leads to the largest value of Eq. (2) with $|\psi_{n'\boldsymbol{k}}^{l'}\rangle \to U_j|\psi_{n'\boldsymbol{k}}^{l'}\rangle$. We also noted that the iteration converges significantly faster if every other gradient ascent step is replaced by performing a $\boldsymbol{k}$-independent update: we sample φ from a Gaussian distribution and generate a symmetrized generator Λ. Only if Eq. (2) with $|\psi_{n'\boldsymbol{k}}^{l'}\rangle \to e^{i\varphi\Lambda}|\psi_{n'\boldsymbol{k}}^{l'}\rangle$ is larger than before, we accept the update. Finally, note that our approach does not require that all paths are identified perfectly and we do not have to perform the path-finding iteration for all combinations of l and l'. Because of the stability to perturbations, it also works if we only iterate for a randomly chosen fraction $f \leq 1$ of pairs of samples, reducing the computational cost.

Altland-Zirnbauer in 1D.—In the remainder, we apply our ML scheme to a variety of symmetry classes. To start, let us consider the AZ classes in 1D and $N_b = 2$-band models. The set of Hamiltonians we want to cluster are of the Kitaev form [58],

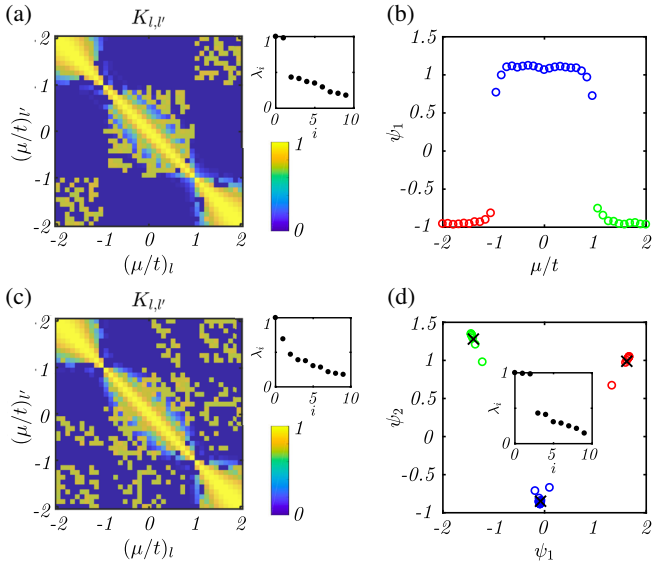

FIG. 2. (a) The kernel and resulting eigenvalues (inset) for the Hamiltonian (5) embedded in class AIII, together with (b) the dominant component ψ_1 as a function of μ/t. (c) is the same as (a) but for class A. For class BDI (d), we have $N_t = 3$ dominant eigenvectors (inset) that reveal three clusters (main panel), where colors refer to values of μ/t as in (b) and the crosses to the k-means centroids. Hyperparameters: $N_k = 50$, $\epsilon = 0.03$, $\eta = 0.3$, $N_{\text{kick}} = 30$, $f = 0.5$.

$$h_k = \Delta \sin k\sigma_1 + (-t\cos k - \mu)\sigma_3. \tag{5}$$

Here σ_j are Pauli matrices and we set $\Delta = t$ such that we are left with only one dimensionless parameter μ/t to parametrize the phase diagram. For topological classification, there are different "ensembles" of Hamiltonians we can embed Eq. (5) in.

Starting with class AIII, we only impose chiral symmetry $C = i\sigma_2$. In Fig. 2(a), we illustrate the resulting kernel associated with the effective graph after searching for additional deformations between the Hamiltonians. We see that the ML procedure correctly identifies that there are adiabatic paths between Hamiltonians with $\mu/t < -1$ and $\mu/t > 1$; note that these paths are not present in the dataset of Hamiltonians nor part of the parametrization (5), as the direct overlap according to the similarity measure (1) is very small between Hamiltonians in Eq. (5) with $\mu/t < -1$ and $\mu/t > 1$. We now take this kernel as input for the ML procedure of [35], which yields a set of eigenvalues λ_i and associated eigenvectors $(\psi_i)_l$, $i = 0, 1, \ldots$. The number N_t of λ_i (exponentially) close to 1 is equal to the number of distinct topological equivalence classes in the data; as expected, we here get $N_t = 2$, see inset in Fig. 2(a), with a clear gap to the subleading eigenvalues. Furthermore, the clustering according to topological features is visible in the low-dimensional embedding $l \to [(\psi_1)_l, \ldots, (\psi_{N_t-1})_l]$. Consequently, in our case here, ψ_1 should be sufficient and, indeed, we see in Fig. 2(b) that ψ_1 correctly identifies the

two topologically distinct regimes $|\mu/t| > 1$ and $|\mu/t| < 1$.

Next, we consider class A, i.e., we do not impose any symmetry. As in any odd dimension, all phases must be equivalent and, indeed, the ML procedure finds paths between all three regimes $\mu/t < -1$, $-1 < \mu/t < 1$, and $\mu/t > 1$, see Fig. 2(c), and there is only one dominant eigenvalue (see inset).

Finally, let us embed Eq. (5) in class BDI, i.e., impose both TRS, $\Theta = i\sigma_3\mathcal{K}$, with complex conjugation $\mathcal{K}$, and PHS, $\Xi = i\sigma_1\mathcal{K}$. As can be seen in Fig. 2(d), we find three quasidegenerate dominant eigenvalues and three clusters in the associated low-dimensional embedding $[\psi_1, \psi_2]$, corresponding to the three phases separated by gap closings at $\mu/t = \pm 1$. Although the stable topological $\mathbb{Z}$-invariant of class BDI is the same for $\mu/t < -1$ and $\mu/t > 1$, this is the correct answer within the subspace of two-band models, see Supplemental Material [54]. To investigate this further, we have taken two identical copies of Eq. (5), yielding a $N_b = 4$-band model; in that case, the ML yields two sectors corresponding $|\mu/t| > 1$ and $|\mu/t| < 1$, as anticipated.

Crystalline symmetries.—To appeal to topological phases stabilized by crystalline symmetries, let us consider the $N_b = 4$-band model

$$h_k = \sin k(a_1\sigma_3 \otimes \tau_1 + a_2\sigma_0 \otimes \tau_2) + [t(1 - \cos k) - m]\sigma_0 \otimes \tau_3 + \Delta t \cos k\sigma_0 \otimes (\tau_0 + \tau_3) + \delta\sigma_1 \otimes \tau_3, \tag{6}$$

where both σ_j and τ_j are Pauli matrices acting in different spaces. This model exhibits inversion symmetry, $Ph_{-k}P^\dagger = h_k$ with $P = \sigma_0 \otimes \tau_3$, which is the only symmetry we impose. We focus on $a_1 = a_2 = t$ and $\delta/t = 2$ in the following. Allowing for gap closings only between the pairs of bands $n = 1, 2$ and $n = 3, 4$, the phase diagram of the approach is shown in Fig. 3(a). We see by comparison with the eigenvalues $\zeta_n^{k_\Theta}$ of P at the Θ-invariant momenta $k_\Theta = 0, \pi$ (right panel), that it correctly identifies that $\zeta_1^0 + \zeta_2^0$ and $\zeta_1^\pi + \zeta_2^\pi$ characterize the distinct topological equivalence classes of band structures [59].

Referencing.—Recent schemes essentially indicate band topology [60,61] by using constraints [5] and comparing to a trivial reference subset, e.g., band structures that can be obtained after Fourier transforming localized real-space Wannier states. Our scheme is flexible to allow for deformations up to an arbitrary reference and, as such, has the potential to prove useful for the identification and characterization of real materials, e.g., in combination with high-throughput *ab initio* studies [62–64]. To exemplify defining trivial reference sets, we consider the 1D model with inversion symmetry in Eq. (6). Note that 1D is special and there is no unique choice for this trivial subset; in analogy to the Su-Schrieffer-Heeger chain, we here choose states without a filling anomaly to be trivial [65–68], which

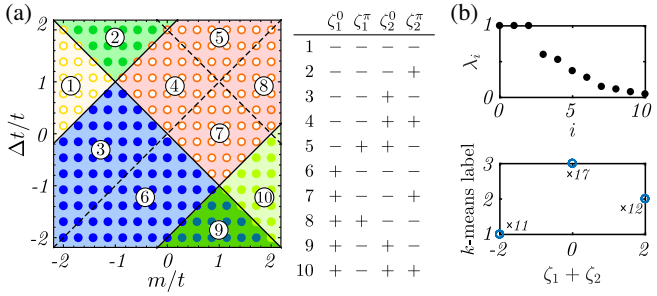

FIG. 3. The colors of the circles in (a) correspond to different k-means labels obtained for $m = 15 \times 14$ samples of Hamiltonians in Eq. (6) from the low-dimensional embedding of our ML procedure ($N_t = 6$ is found). Filled (empty) circles correspond to Hamiltonians not connected (connected) to a trivial atomic insulator. The table (right) shows the eigenvalues of P of the phase diagram. (b) Sampling $m = 40$ trivial insulators, we identify three different classes (see eigenvalues, upper) correlated with $\zeta_1 + \zeta_2$ (scatterplot k means vs $\zeta_1 + \zeta_2$, lower). We use $N_k = 50$, $\epsilon = 0.03$, $\eta = 0.8$, $N_{\text{kick}} = 0$, $f = 0.2$ (a), $f = 0.5$ (b).

amounts to taking the set of momentum-independent, inversion symmetric Hamiltonians as reference, see Supplemental Material [54]. As a first step, we randomly sample momentum-independent Hamiltonians with inversion symmetry and apply our ML procedure to classify them. As can be seen in Fig. 3(b), we find the correct number of three different equivalence classes, which correspond to the net parity $\zeta_1 + \zeta_2$, with $\zeta_n \equiv \zeta_n(0) = \zeta_n(\pi)$. As a second step, we take one member of each of those three classes of trivial states and add them to set of Hamiltonians of Fig. 3(a). This allows us to determine which of the phases in the phase diagram are adiabatically connected to a trivial reference set (open circles) and, thus, trivial, and which are not (solid circles, topological).

Two dimensions.—To illustrate higher dimensions, we discuss the Bernevig-Hughes-Zhang (BHZ) model [69],

$$h_{\boldsymbol{k}} = a_1 \sin(k_x)\Gamma_x + a_2 \sin(k_y)\Gamma_y + M_{\boldsymbol{k}}\Gamma_0, \tag{7}$$

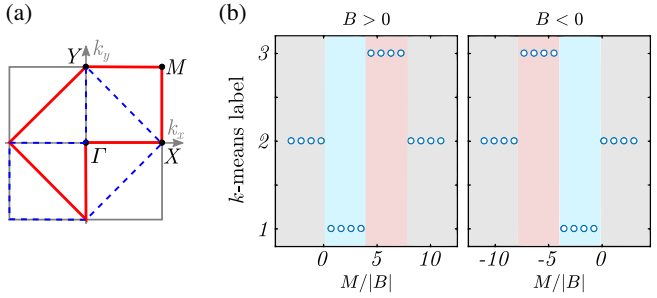

FIG. 4. (a) 1D closed path in the Brillouin zone (red solid) going through the indicated high-symmetry points and its time-reversal partner (blue dashed) that, due to symmetry, is effectively also taken into account. (b) k-means labels for the BHZ model (7) as a function of M for $B > 0$ (left) and $B < 0$ (right). Hyperparameters: $N_k = 180$, $\epsilon = 0.05$, $\eta = 0.4$, $N_{\text{kick}} = 50$, $f = 0.5$.

where $M_{\boldsymbol{k}} = M - 2B[2 - \cos(k_x) - \cos(k_y)]$, $\Gamma_x = \sigma_3 \otimes \tau_1$, $\Gamma_y = \sigma_0 \otimes \tau_2$, and $\Gamma_0 = \sigma_0 \otimes \tau_3$. We focus on $a_1 = a_2 = |B|$ and only impose TRS with $\Theta = i\sigma_2 \otimes \tau_0 \mathcal{K}$ as symmetry. As discussed, we do not have to take into account all 2D momenta, but can focus on paths that go through all high-symmetry momenta; for the BHZ model with TRS, the latter are Γ, X, Y, and M [5], and we will take the path shown in red in Fig. 4(a). To test our ML approach, we take BHZ Hamiltonians with different values of $M/|B|$ for both signs of B as input. As can be seen in Fig. 4(b), it finds the nontrivial paths between Hamiltonians with opposite signs of B and identifies the three topologically distinct phases [70,71].

Conclusion.—We presented a ML algorithm that identifies adiabatic paths between Hamiltonians, readily applicable to any arbitrary symmetry class, thereby allowing one to construct topological phase diagrams without supervision. We expect that future work based on reinforcement or in combination with supervised learning can further improve our approach. Because of the flexibility of the algorithm, which we hope to also prove useful in the study of interacting systems, it has the potential to deepen our understanding of topological phases.

In particular, we thank Joaquin Rodriguez-Nieva for an inspiring previous collaboration [35] and for useful comments on this work. We further thank Henry Shackleton for useful discussions. M. S. S. acknowledges support from the National Science Foundation under Grant No. DMR-1664842. R. J. S. appreciatively acknowledges funding via Ashvin Vishwanath at Harvard University, Trinity College of the University of Cambridge, and the Winton Programme at the University of Cambridge.

Note added.—Recently, another work [72] appeared on arXiv. In that work, phononic systems were clustered, applying the procedure of [35] directly to randomly sampled models, rather than combining it with an explicit path-finding approach as we propose here. The latter is required to explore the full space of deformations in a given symmetry class.

[1] X.-L. Qi and S.-C. Zhang, Rev. Mod. Phys. **83**, 1057 (2011).
[2] M. Z. Hasan and C. L. Kane, Rev. Mod. Phys. **82**, 3045 (2010).
[3] L. Fu, Phys. Rev. Lett. **106**, 106802 (2011).
[4] R.-J. Slager, A. Mesaros, V. Juričić, and J. Zaanen, Nat. Phys. **9**, 98 (2013).
[5] J. Kruthoff, J. de Boer, J. van Wezel, C. L. Kane, and R.-J. Slager, Phys. Rev. X **7**, 041069 (2017).
[6] D. S. Freed and G. W. Moore, Ann. Henri Poincaré **14**, 1927 (2013).
[7] V. Dunjko and H. J. Briegel, Rep. Prog. Phys. **81**, 074001 (2018).
[8] S. Das Sarma, D.-L. Deng, and L.-M. Duan, Phys. Today **72**, No. 3, 48 (2019).
[9] P. Mehta, M. Bukov, C.-H. Wang, A. G. Day, C. Richardson, C. K. Fisher, and D. J. Schwab, Phys. Rep. **810**, 1 (2019).
[10] G. Carleo, I. Cirac, K. Cranmer, L. Daudet, M. Schuld, N. Tishby, L. Vogt-Maranto, and L. Zdeborová, Rev. Mod. Phys. **91**, 045002 (2019).
[11] G. Carleo and M. Troyer, Science **355**, 602 (2017).
[12] R. G. Melko, G. Carleo, J. Carrasquilla, and J. I. Cirac, Nat. Phys. **15**, 887 (2019).
[13] J. Liu, Y. Qi, Z. Y. Meng, and L. Fu, Phys. Rev. B **95**, 041101(R) (2017).
[14] G. R. Schleder, A. C. M. Padilha, C. M. Acosta, M. Costa, and A. Fazzio, J. Phys. Mater. **2**, 032001 (2019).
[15] J. Schmidt, M. R. G. Marques, S. Botti, and M. A. L. Marques, npj Comput. Mater. **5**, 83 (2019).
[16] M. Klintenberg, J. T. Haraldsen, and A. V. Balatsky, Appl. Phys. Res. **6**, 31 (2014).
[17] G. Cao, R. Ouyang, L. M. Ghiringhelli, M. Scheffler, H. Liu, C. Carbogno, and Z. Zhang, Phys. Rev. Mater. **4**, 034204 (2020).
[18] N. Claussen, B. A. Bernevig, and N. Regnault, arXiv:1910.10161.
[19] V. Peano, F. Sapper, and F. Marquardt, arXiv:1912.03296.
[20] J. Robledo Moreno, G. Carleo, and A. Georges, arXiv:1911.03580.
[21] J. Carrasquilla and R. G. Melko, Nat. Phys. **13**, 431 (2017).
[22] L. Wang, Phys. Rev. B **94**, 195105 (2016).
[23] K. Ch'ng, J. Carrasquilla, R. G. Melko, and E. Khatami, Phys. Rev. X **7**, 031038 (2017).
[24] Y. Zhang and E.-A. Kim, Phys. Rev. Lett. **118**, 216401 (2017).
[25] Y. Zhang, R. G. Melko, and E.-A. Kim, Phys. Rev. B **96**, 245119 (2017).
[26] E. P. L. van Nieuwenburg, Y.-H. Liu, and S. D. Huber, Nat. Phys. **13**, 435 (2017).
[27] D.-L. Deng, X. Li, and S. D. Sarma, Phys. Rev. B **96**, 195145 (2017).
[28] Y.-T. Hsu, X. Li, D.-L. Deng, and S. D. Sarma, Phys. Rev. Lett. **121**, 245701 (2018).
[29] N. Yoshioka, Y. Akagi, and H. Katsura, Phys. Rev. B **97**, 205110 (2018).
[30] P. Zhang, H. Shen, and H. Zhai, Phys. Rev. Lett. **120**, 066401 (2018).
[31] N. Sun, J. Yi, P. Zhang, H. Shen, and H. Zhai, Phys. Rev. B **98**, 085402 (2018).
[32] D. Carvalho, N. A. García-Martínez, J. L. Lado, and J. Fernández-Rossier, Phys. Rev. B **97**, 115453 (2018).
[33] I. A. Iakovlev, O. M. Sotnikov, and V. V. Mazurenko, Phys. Rev. B **98**, 174411 (2018).
[34] W. Hu, R. R. P. Singh, and R. T. Scalettar, Phys. Rev. E **95**, 062122 (2017).
[35] J. F. Rodriguez-Nieva and M. S. Scheurer, Nat. Phys. **15**, 790 (2019).
[36] P. Huembeli, A. Dauphin, and P. Wittek, Phys. Rev. B **97**, 134109 (2018).
[37] N. L. Holanda and M. A. R. Griffith, arXiv:1901.01963.
[38] T. Ohtsuki and T. Mano, J. Phys. Soc. Jpn. **89**, 022001 (2020).

[39] M. D. Caio, M. Caccin, P. Baireuther, T. Hyart, and M. Fruchart, arXiv:1901.03346.
[40] Y. Ming, C.-T. Lin, S. D. Bartlett, and W.-W. Zhang, npj Comput. Math. **5**, 88 (2019).
[41] Y.-H. Tsai, M.-J. Yu, Y.-H. Hsu, and M.-C. Chung, arXiv:1909.04784.
[42] F. Schäfer and N. Lörch, Phys. Rev. E **99**, 062107 (2019).
[43] E. Greplova, A. Valenti, G. Boschung, F. Schäfer, N. Lörch, and S. Huber, New J. Phys. **22**, 045003 (2020).
[44] W. Lian, S.-T. Wang, S. Lu, Y. Huang, F. Wang, X. Yuan, W. Zhang, X. Ouyang, X. Wang, X. Huang, L. He, X. Chang, D.-L. Deng, and L. Duan, Phys. Rev. Lett. **122**, 210503 (2019).
[45] O. Balabanov and M. Granath, Phys. Rev. Research **2**, 013354 (2020).
[46] M. J. S. Beach, A. Golubeva, and R. G. Melko, Phys. Rev. B **97**, 045207 (2018).
[47] R. R. Coifman, S. Lafon, A. B. Lee, M. Maggioni, B. Nadler, F. Warner, and S. W. Zucker, Proc. Natl. Acad. Sci. U.S.A. **102**, 7426 (2005).
[48] S. Sachdev, Rep. Prog. Phys. **82**, 014001 (2019).
[49] A. Y. Kitaev, Ann. Phys. (Amsterdam) **303**, 2 (2003).
[50] A. Bouhon, R.-J. Slager, and T. Bzdusek, arXiv:1907.10611.
[51] H. C. Po, H. Watanabe, and A. Vishwanath, Phys. Rev. Lett. **121**, 126402 (2018).
[52] A. Bouhon, A. M. Black-Schaffer, and R.-J. Slager, Phys. Rev. B **100**, 195135 (2019).
[53] R.-J. Slager, L. Rademaker, J. Zaanen, and L. Balents, Phys. Rev. B **92**, 085126 (2015).
[54] See Supplemental Material at http://link.aps.org/supplemental/10.1103/PhysRevLett.124.226401 for details on explicit deformations of 1D models, referencing in 1D and beyond, steepest ascent and symmetrization, and cutoff dependence.
[55] This symmetrization is consistent with the steepest ascent condition used to derive Eq. (3) [54].
[56] A. Alexandradinata, X. Dai, and B. A. Bernevig, Phys. Rev. B **89**, 155114 (2014).
[57] R. Yu, X. L. Qi, A. Bernevig, Z. Fang, and X. Dai, Phys. Rev. B **84**, 075119 (2011).
[58] A. Y. Kitaev, Phys. Usp. **44**, 131 (2001).
[59] T. L. Hughes, E. Prodan, and B. A. Bernevig, Phys. Rev. B **83**, 245132 (2011).
[60] H. C. Po, A. Vishwanath, and H. Watanabe, Nat. Commun. **8**, 50 (2017).
[61] B. Bradlyn, L. Elcoro, J. Cano, M. G. Vergniory, Z. Wang, C. Felser, M. I. Aroyo, and B. A. Bernevig, Nature (London) **547**, 298 (2017).
[62] T. Zhang, Y. Jiang, Z. Song, H. Huang, Y. He, Z. Fang, H. Weng, and C. Fang, Nature (London) **566**, 475 (2019).
[63] M. G. Vergniory, L. Elcoro, C. Felser, N. Regnault, B. A. Bernevig, and Z. Wang, Nature (London) **566**, 480 (2019).
[64] F. Tang, H. C. Po, A. Vishwanath, and X. Wan, Nat. Phys. **15**, 470 (2019).
[65] Y. Hwang, J. Ahn, and B.-J. Yang, Phys. Rev. B **100**, 205126 (2019).
[66] N. Read, Phys. Rev. B **95**, 115309 (2017).
[67] A. Alexandradinata, J. Holler, C. Wang, H. Cheng, and L. Lu, arXiv:1908.08541.
[68] W. A. Benalcazar, T. Li, and T. L. Hughes, Phys. Rev. B **99**, 245151 (2019).
[69] B. A. Bernevig, T. L. Hughes, and S.-C. Zhang, Science **314**, 1757 (2006).
[70] V. Juričić, A. Mesaros, R.-J. Slager, and J. Zaanen, Phys. Rev. Lett. **108**, 106403 (2012).
[71] R.-J. Slager, J. Phys. Chem. Solids **128**, 24 (2019).
[72] Y. Long, J. Ren, and H. Chen, Phys. Rev. Lett. **124**, 185501 (2020).